Available online at www.sciencedirect.com
ScienceDirect
Journal of Power Sources 181 (2008) 363–370
JOURNAL OF POWER SOURCES
www.elsevier.com/locate/jpowsour

An experimental study of a PEM fuel cell power train for urban bus application

P. Corbo *, F. Migliardini, O. Veneri

Istituto Motori, National Research Council (CNR), Italy

Received 26 September 2007; received in revised form 30 October 2007; accepted 31 October 2007
Available online 20 February 2008

Abstract

An experimental study was carried out on a fuel cell propulsion system for minibus application with the aim to investigate the main issues of energy management within the system in dynamic conditions. The fuel cell system (FCS), based on a 20 kW PEM stack, was integrated into the power train comprising DC–DC converter, Pb batteries as energy storage systems and asynchronous electric drive of 30 kW. As reference vehicle a minibus for public transportation in historical centres was adopted. A preliminary experimental analysis was conducted on the FCS connected to a resistive load through a DC–DC converter, in order to verify the stack dynamic performance varying its power acceleration from 0.5 kW s^{-1} to about 4 kW s^{-1}. The experiments on the power train were conducted on a test bench able to simulate the vehicle parameters and road characteristics on specific driving cycles, in particular the European R40 cycle was adopted as reference. The "soft hybrid" configuration, which permitted the utilization of a minimum size energy storage system and implied the use of FCS mainly in dynamic operation, was compared with the "hard hybrid" solution, characterized by FCS operation at limited power in stationary conditions. Different control strategies of power flows between fuel cells, electric energy storage system and electric drive were adopted in order to verify the two above hybrid approaches during the vehicle mission, in terms of efficiencies of individual components and of the overall power train.

The FCS was able to support the dynamic requirements typical of R40 cycle, but an increase of air flow rate during the fastest acceleration phases was necessary, with only a slight reduction of FCS efficiency. The FCS efficiency resulted comprised between 45 and 48%, while the overall power train efficiency reached 30% in conditions of constant stack power during the driving cycle.

Keywords: Fuel cells; Power train; Electric vehicles; Energy management

1. Introduction

It is widely accepted that the climate changes due to greenhouse effects could be mainly attributed to anthrop activities based on the combustion of fossil fuels. The CO_2 concentration in the earth atmosphere progressively increases (today its mean value is about 400 ppm) and could reach in few decades a very dangerous value of 700 ppm in the absence of any hindering intervention. On the other hand, the conventional oil production will peak within 20 years (the natural gas production will peak 10–20 years later), while world energy consumption continues to grow at 2% per annum [1]. In this context it is strongly justified the growing interest towards the potential benefits associated to the so-called "hydrogen economy", because a wide diffusion of hydrogen as energy vector would permit the development of a global energy strategy based on a massive utilization of different primary sources including renewable (solar and wind) and/or nuclear [2]. Furthermore, as the transportation sector depends almost totally on oil, it seems really urgent to individuate a mid-long-term solution able to guarantee the future mobility of citizens paying respect to environmental and energy saving issues.

Polymeric electrolyte fuel cells (PEFC) make really interesting the utilization of hydrogen in the field of transportation systems because they are characterized by working conditions at low temperature, high efficiency, high performances in a wide working zone and very good dynamic characteristics [3–5]. In particular the utilization of PEFC would permit to maintain the principal advantages of electric vehicles, overcoming their main limitations, i.e. very low vehicle range and long time for

* Corresponding author. Tel.: +39 0817177180; fax: +39 0812396097.
E-mail address: p.corbo@im.cnr.it (P. Corbo).

0378-7753/$ – see front matter © 2007 Elsevier B.V. All rights reserved.
doi:10.1016/j.jpowsour.2007.10.089

recharging batteries. In particular, the main advantages of a fuel cell propulsion system are the following:

- the PEFC hydrogen fuel cells represent a very efficient energy conversion system, for this reason they contribute to the realization of very high efficient propulsion systems.
- the electrochemical reaction outlets are water, heat and electric energy, so there are no harmful emissions, which represent a critical issue for internal combustion engines.
- the vehicle autonomy is increased and depends on the quantity of hydrogen stored on board. Actually hydrogen storage issues represent a critic point in order to practically apply fuel cell propulsion systems but many promising progresses have been made in the last years [6,7].
- the recharging times can be strongly shorter with respect to batteries, as they depend on the characteristics of the fuel storage system.

The current status of the fuel cell technology confirms its high potential in terms of efficiency especially for application in passenger cars [8,9], even if many progresses are required for reducing costs and improving reliability in dynamic conditions. As a consequence fuel cell vehicles at the present development stage suffer of high prices and short life times, which make their commercialization on wide scale not expectable in few years [10,11].

A fuel cell propulsion system can be developed using the fuel cells as "full power", without the support of batteries, or in hybrid configuration, where the storage systems play an important role in defining the power management and the fuel cells can operate with an accurate control of their dynamics [12–14]. A "soft hybrid" configuration permits to minimize the contribution of storage system with a positive impact on vehicle weight and size, while a "hard hybrid" layout increases the energy capacity and then the size of storage systems, but reduces the contribution of fuel cells, which can be chosen with a nominal power lower than the maximum electric drive power, with significant advantages in terms of costs [15,16].

The design of the fuel cell power train and the definition of the proper control strategies for efficiency optimization require an analysis of fuel cell system (FCS) dynamic performance [17,18], which has to be carried out in experimental conditions close to those encountered in real applications. In particular, the main issues to be considered refer to the interaction between air compressor and stack [19], and to purge and humidification strategies [20–22].

The current open scientific literature hardly reports experimental works regarding hybrid fuel cell power trains, especially in real conditions of a vehicle utilization. Most results have been obtained in modeling field, regarding both different power train components and the overall propulsion system [23–25]. The aim of this work was the experimental characterization of a 30 kW fuel cell power train for minibus applications in dynamic conditions characteristic of road utilization. In particular the propulsion system was powered in hybrid configuration by Pb batteries and 20 kW PEM stack, and the experimental tests were carried out on laboratory test bench utilizing the European R40 driving cycle as dynamic load demand. Both soft and hard hybrid configurations were analyzed as function of different load variation rates, and for each control strategy the efficiencies of the overall power train and individual sub-systems were evaluated. The interaction between stack and its auxiliary components in dynamic conditions was investigated to address the choice of hybridization level.

2. Experimental

A 20 kW PEM stack was integrated with all auxiliary components necessary to its management. Hydrogen as fuel and nitrogen necessary for cell and hydrogen pipeline purge were fed by high pressure cylinders (200 bar) of high purity (>99.5%), while a pressure reduction stage (7 bar maximum) was installed at hydrogen inlet. The PEM stack operated in all experimental tests in dead-end configuration, i.e. anodic compartment was maintained closed and pressurized. A purge electric valve was inserted at hydrogen line outlet to drain excess of water diffusing from cathode to anode side through the polymeric membrane.

A low pressure (below 130 kPa) side channel compressor was used for tests. The humidification was realized by flowing air through a bubbler filled with de-ionized water. This was heated at different temperatures by an electric resistance before feeding the cathode side. Humidification and temperature sensors at cathode inlet permitted air relative humidity to be controlled. Stack temperature was measured by a thermocouple at the outlet of cathode side. The air flow rate was regulated by acting on the speed control of the compressor motor controller and measured by a variable-area flowmeter in order to assure the necessary stoichiometric ratio. This is defined as $R = R_{\text{eff}}/R_{\text{stoich}}$ where R_{eff} is the ratio between the air and hydrogen mass flow rates, while R_{stoich} is the same ratio as required by the stoichiometric equation of H_2 oxidation. Two pressure transducers were located upstream the stack to monitor anode and cathode pressure during the experimental runs. Inlet hydrogen pressure was maintained higher of 30 kPa with respect to inlet air pressure during all experimental tests. A water condenser was inserted at the stack outlets before vent to verify the water balance in the system. The cooling system, adopted to control the temperature in the range 290–346 K, was constituted by a de-ionized water circuit equipped by pump and sensors for pressure, temperatures and flow rate. In order to assure an approximately uniform temperature through the cells, a difference not higher than 5 K was maintained between inlet and outlet cooling water temperatures. This was achieved by imposing the cooling water flow rate at the value required by the maximum stack power ($4\,m^3\,h^{-1}$). A spiral heat exchanger fed with external water was used to control the cooling water temperature.

The hydrogen purge, external humidification and stack temperature strategies were selected with the criterion of minimizing the energy consumption of auxiliary components, and were maintained unvaried during all experiments [26]. Defining the fuel utilization coefficient (η_{util}) as ratio between mass of fuel reacted in the stack and mass of fuel entering the stack, the selected purge strategy maintained this parameter at the constant value of 0.90.

Regarding stack humidification the inlet air was saturated at room temperature (290–300 K), in order to minimize the external contribution to the optimal membrane hydration and reduce the electric consumption of the humidifier and the purge frequency [19]. As a consequence, the stack temperature was maintained at about 315 K, in order to avoid membrane dehydration.

A dedicated acquisition system able to monitor and register the voltage of the individual cells during the different runs was adopted. A d-Space board was used for acquisition and control of all signals associated to FCS components (valves, sensors, transducers).

An IGBT DC–DC converter of 20 kW was interconnected between the fuel cell system and the electric load to adapt the variable stack voltage to the load electric voltage. The DC–DC converter outlet was firstly connected to a variable resistive load of maximum 20 kW for the fuel cell characterization, then to the electric bus of the power train. The DC–DC converter was equipped with current and voltage sensors to evaluate instantaneously the electric power flow between the fuel cell system and the electric load or the power train. It was controlled by the d-Space board, which was programmed to follow the desired stack current reference during the tests.

The test bench for power train characterization was composed by a 120 kW dynamic electric brake constituted by a three-phase asynchronous machine and appropriate converters, which provide a bidirectional flow of the energy with respect to the electric network. The power train test bench could be easily reconfigured by software for testing different types of vehicles, driving cycles, rolling resistances and aerodynamic drags.

The 30 kW electric drive for road applications was composed by an asynchronous machine and an IGBT inverter, both with water cooling system. The 6000 rpm maximum motor speed was reduced by means a gear box which only provided the forward and reverse gear. A Pb battery pack was used as storage system, composed by 24 batteries connected in series. Each single battery was characterized by a nominal voltage of 12 V and an electric capacity of 50 Ah. The battery pack was also provided with an electric switch for its connection or disconnection to the power train.

The electric drive, the DC–DC converter and the Pb battery pack were equipped with sensors able to monitor all the main parameters of the electric power train during the tests. All the analogic and digital signals were connected to a d-SPACE prototyping system, which integrated The MathWorks' MATLAB development tools.

The European R40 driving cycle (Fig. 1) is composed by three phases, the first two being characterized by acceleration, constant speed and deceleration steps, while the last one presents two steps at constant, before returning to zero speed. It was used in this work to evaluate the performance of the fuel cell power train on a typical urban route.

3. Results and discussion

A preliminary experimental analysis was carried out on the FCS connected to a variable resistive load through the DC–DC converter, which permitted to simulate the instantaneous current requests of electric drive during the European R40 driving cycle. The analysis was performed varying the slope of the acceleration phases (between 5 and 50 A s^{-1} as stack current requirements), and drawing for each condition indications about the dynamic stack performance from the examination of individual cell voltage during the transient step.

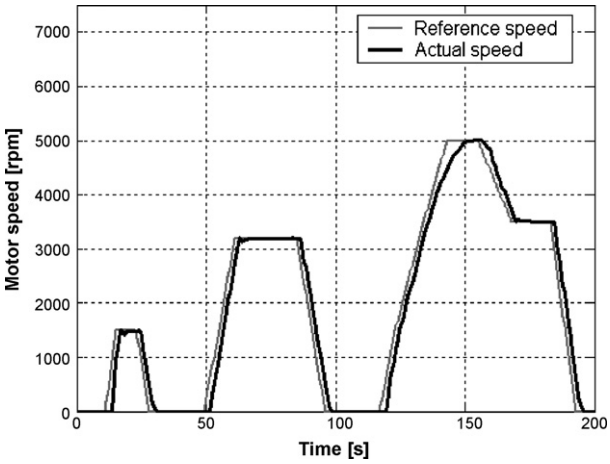

Fig. 1. Profile of motor speed vs. time for the European R40 driving cycle.

The results derived from this investigation were then utilized in designing of power train control strategies on the same R40 driving cycle. In particular, experimental tests were conducted on the test bench varying both dynamics and maximum power of the test cycle for different hybridization levels between FCS and batteries.

3.1. Dynamic investigation of the 20 kW FCS on R40 cycle

The first experiment on the FCS connected to the resistive load was conducted utilizing as test cycle the R40 simplified to have just three neat peaks and modified in order to obtain accelerations phases of 5 A s^{-1} in terms of current requirements and maximum power of about 10 kW. The values of air flow rate were preliminarily regulated in steady state conditions for all the load range comprised in the test cycle, in order to assure the

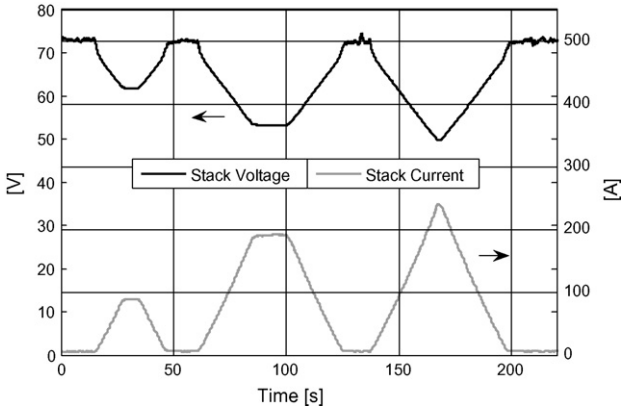

Fig. 2. Stack voltage and current vs. time for dynamic test at 5 A s^{-1} based on the R40 cycle.

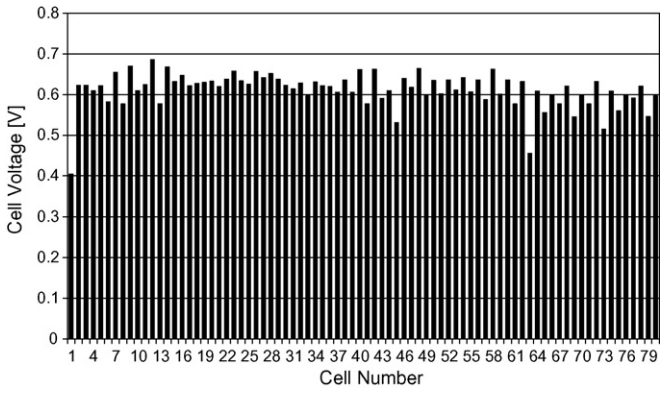

Fig. 3. Individual cell voltage acquisition during the experiment of Fig. 2 at $t = 170$ s (240 A).

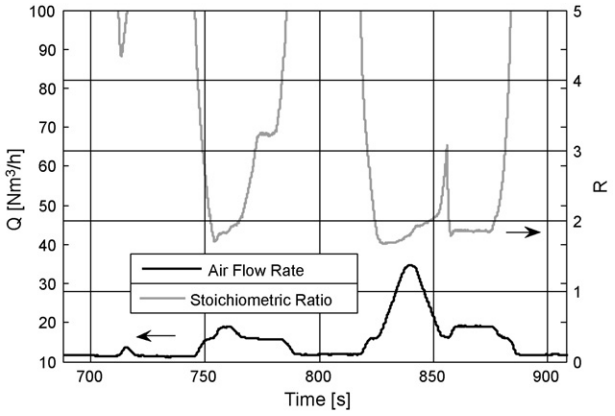

Fig. 5. Stoichiometric ratio and air flow rate vs. time for the experiment of Fig. 4.

minimum power consumption of the air compressor compatible with satisfactory cell voltages. In particular a compressor control strategy was adopted to maintain R values equal to 1.8 in the range 100–240 A, and to let them drop from 6 to 2 from open circuit to 100 A. In Fig. 2 the stack current and voltage measured during this test are reported as function of cycle length. The stack voltage reached the minimum values of 63, 52 and 48 V in correspondence of three current peaks of 80, 180 and 240 A, respectively. The R values reproduced the steady state settings with minimum $R = 1.8$, while air flow rate reached 35 $m^3\,h^{-1}$ at 240 A. The stack voltage profiles in Fig. 2 are in agreement with data of the polarization curve obtained on the same stack, reported elsewhere [19], suggesting that the dynamic of 5 A s^{-1} does not interfere with the regular stack operation, as confirmed by the analysis of individual cell voltage, shown in Fig. 3 for the instant corresponding to 240 A. In particular, it can be noticed that most cells showed a voltage close to 0.6 V, while a voltage decrease was measured only for the first cell (about 0.4 V) and in the last group of 20 cells, where values comprised between 0.45 and 0.55 V were detected for few cells. As expectable, the behaviour of these cells resulted better for all the other current values. Since no cell during the test decreased under 0.4 V, the data therein reported are a general indication that the dynamic considered is satisfactorily supported by the FCS for the cycle utilized.

The R40 cycle was then modified to obtain acceleration phases of 10 A s^{-1}, and another experiment was conducted on this cycle according to the criterion of minimizing the compressor consumption. The results are reported in Fig. 4, where stack current and voltage are shown as function of cycle length, while R and air flow profiles are plotted in Fig. 5. Only a slight voltage decrease was observed in correspondence of the main current peaks (130 and 230 A) with respect to steady state values. The compressor control law permitted to obtain R values only slightly lower than 1.8 for a short transient time at the end of acceleration phases, with air flow rate up to 35 $m^3\,h^{-1}$ at about 230 A. In fact, Fig. 6, where the individual cell voltage acquisition is plotted as function of cycle length, evidences a general slight decrease of all cell voltages, with the first one under 0.5 V already for the second peak current (130 A) and under 0.4 V in correspondence of the highest current peak (230 A). The FCS behaviour at 10 A s^{-1} suggests that at higher current rising rates the dynamic performance requires some modification in management strategies. This was confirmed by the experiment of Figs. 7–10, where a simple dynamic current cycle was used with the same compressor management strategy of the experiment of Fig. 5. This cycle was characterized by an acceleration ramp of 50 A s^{-1}, a short stationary phase at 220 A and a deceleration step at the same rate of acceleration. In Fig. 7 the acquisitions of the current cycle is reported together with the total stack voltage. This dropped down from 71 to about 45 V at the end of

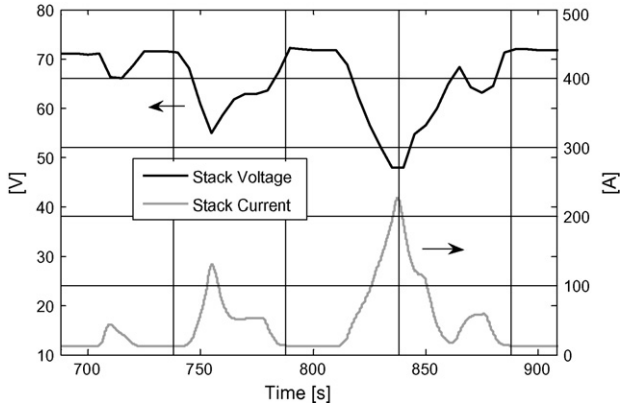

Fig. 4. Stack voltage and current vs. time for dynamic test at 10 A s^{-1} based on the R40 cycle.

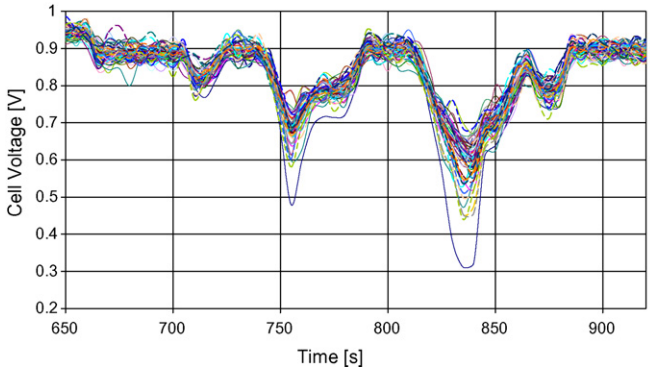

Fig. 6. Individual cell voltage acquisition vs. cycle length during the experiment of Fig. 4.

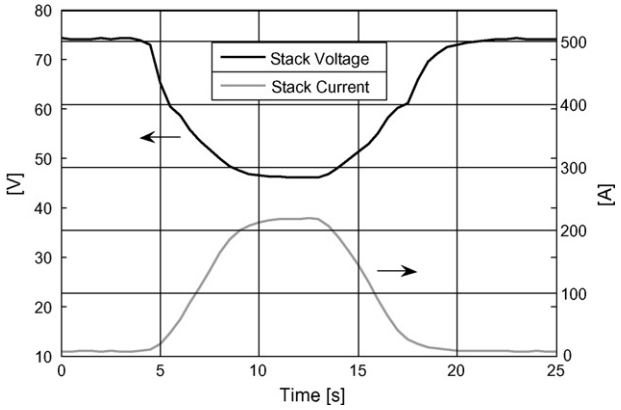

Fig. 7. Stack voltage and current vs. time for dynamic test at 50 A s^{-1}.

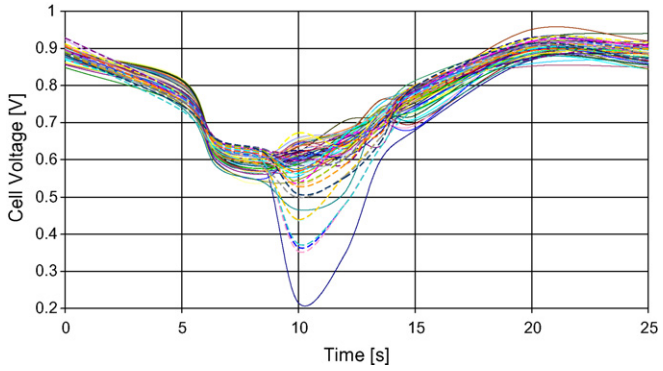

Fig. 9. Individual cell voltage acquisition vs. cycle length during the experiment of Fig. 7.

the acceleration step, then remained constant during the stationary phase (5 s), and rose again during the deceleration step. The *R* and air flow rate profiles (Fig. 8) evidenced that for the high dynamic adopted the compressor working was stressed, in particular the faster dynamic of this test determined an appreciable effect on the stoichiometric ratio, whose profile decreased below 1.5 at the end of the acceleration phase. This behaviour is further evidenced in Figs. 9 and 10, where the individual cell voltages are reported as function of cycle length and as histogram acquired at the instant corresponding to the highest current peak, respectively. An evident problem of stack malfunctioning was evidenced for several cells, in particular the first one dropped under 0.3 V, while other three cells among the last 20 did not reached 0.4 V. This behaviour was attributed to difficulties of air compressor in assuring the necessary stoichiometric ratio values (Fig. 8), and suggested to change the air compressor strategy in order to increase *R* values during the fastest dynamic phases. Figs. 11–14 show the results of a test effected on the R40 cycle operating at 50 A s^{-1} during the acceleration phases, but modified regarding the maximum power, which was limited to the optimal power obtainable by the stack in the experimental condition adopted (12 kW with respect to 25 kW required by the cycle). For this test the air management strategy was modified, in particular air flow rate was increased in the range 0–200 A.

In Fig. 11 the stack current and voltage are reported as function of cycle length, while Fig. 12 shows the corresponding *R* and air flow rate values realized with the modified air management strategy. The voltage profile resulted acceptable during the entire cycle duration, with values never inferior to 47 V, while *R* values did not decreased under 1.8 also during the fastest acceleration phases. The analysis of individual cells (Figs. 13 and 14) confirmed the benefits of the new air management strategies on the stack dynamic behaviour, in particular most cells showed a regular working in the entire load range, while only for some cells a significant voltage diminution was observed at the end of the acceleration phases, with a partial voltage recovery during the stationary phases. No cell dropped under 0.4 V, except for the first one whose voltage decreased at about 0.3 V, confirming the trend already observed at 10 A s^{-1}.

3.2. Fuel cell power train on R40 cycle

The realization and management of a fuel cell propulsion system for road transport application requires the choice of the hybridization level between storage system and FCS. In particular, in a fuel cell power train the batteries can be either minimized committing to the fuel cell stack the task of generating most energy demanded by the load (soft hybrid), or sized in order to provide all vehicle dynamic requirements allowing the utilization of a smaller FCS (hard hybrid). The main benefit of the

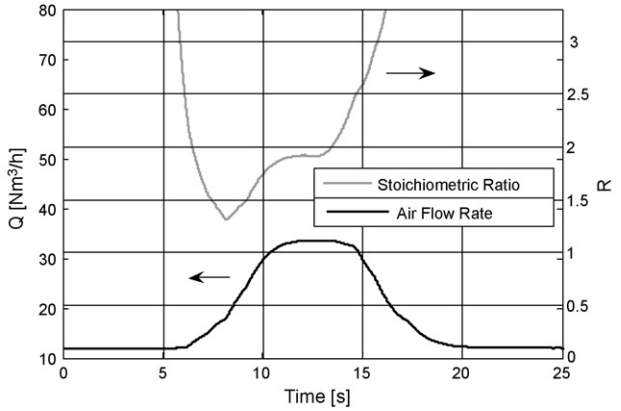

Fig. 8. Stoichiometric ratio and air flow rate vs. time for the experiment of Fig. 7.

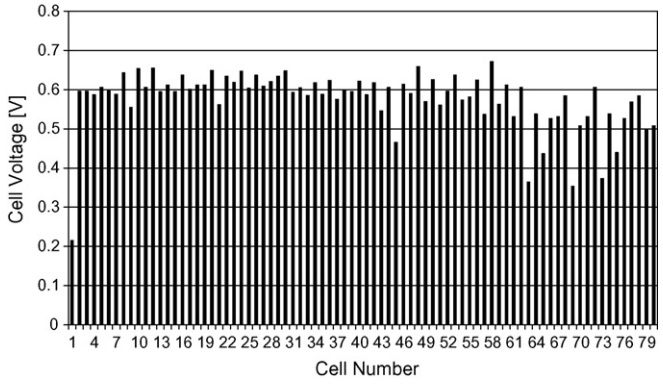

Fig. 10. Individual cell voltage acquisition during the experiment of Fig. 7 at the instant of maximum acceleration (t = 10 s, 220 A).

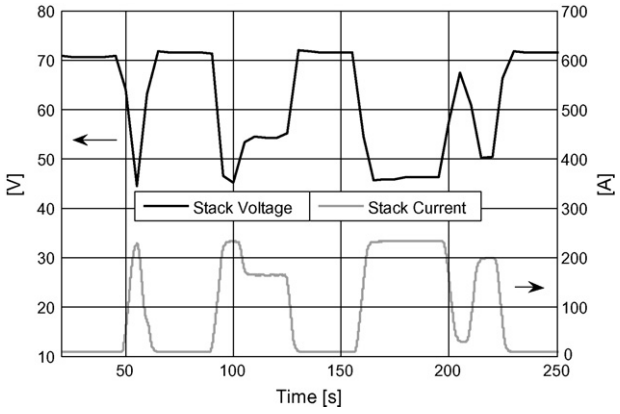

Fig. 11. Stack voltage and current vs. time for dynamic test at 50 A s^{-1} based on the R40 cycle.

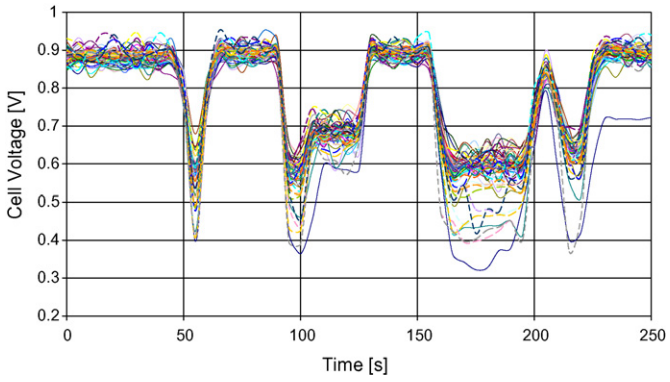

Fig. 13. Individual cell voltage acquisition vs. cycle length during the experiment of Fig. 11.

soft hybrid option is the minor use of the batteries, which could have the minimum capacity necessary to feed the vehicle auxiliaries, give a limited contribution to peak powers and allow some energy economy during regenerative braking. On the other hand, the hard hybrid solution offers the possibility to limit the cost of FCS which could also work in optimal reliability conditions (steady state working). In this context the dynamic performance of the FCS is a further critical aspect to be considered for the definition of proper control strategy of the fuel cell power train.

According to considerations exposed in Section 3.1 the experiments on the overall power train were effected varying the slope of the acceleration phases in the R40 cycle and its maximum power demands. All runs were carried out maintaining the battery SOC at a partial level with respect to nominal battery capacity during the driving cycle, and recovering braking energy as much as possible.

The first experiment on the fuel cell power train was conducted imposing to the R40 cycle an acceleration slope corresponding to the stack current variation profile of Fig. 2 (5 A s^{-1}) and air management strategy of Fig. 5 (minimum compressor consumption). The results are shown in Fig. 15, where the power distribution between engine, battery pack and DC–DC converter is reported versus cycle length. The engine power reaches its three maximum values (5, 10 and 15 kW) at the end of the three acceleration phases of the R40 cycle, then after the stationary phases diminishes up to negative power values during the deceleration phases, when the engine operates as generator. The control strategy adopted for this tests was based on the hypothesis to utilize the hybrid vehicle as pure electric vehicle at the start up and for partial loads, in particular the energy flows inside the power train were regulated to satisfy the engine requirements only by batteries up to about half engine maximum power. For higher loads the FCS supported the engine demands following the same dynamic of the cycle, and recharged the batteries (Fig. 15). The results of Section 3.1 guaranteed that no dynamic limitation could be expected during this experiment. The batteries were recharged during both deceleration phases (regenerative braking) and stationary phase during which the FCS power overcame the engine demands. The behaviour of battery power affected its state of charge during the cycle, for a single R40 cycle managed according to Fig. 15 a slight decrease of battery state of charge (SOC) was observed at the end of the test (about 0.2%). In Table 1 the efficiencies calculated for the power train and its main components on R40 cycle are reported. The total efficiency of the fuel cell system (η_{FCS}) was calculated as the ratio between the power at DC–DC converter input and the theoretical power associated to the fuel entering the stack. The DC–DC converter (η_{DC}) and electrical drive (η_{ED}) efficiencies were calculated as ratio between outlet and inlet power of the devices. Then the total efficiency of the power train (η_{PT})

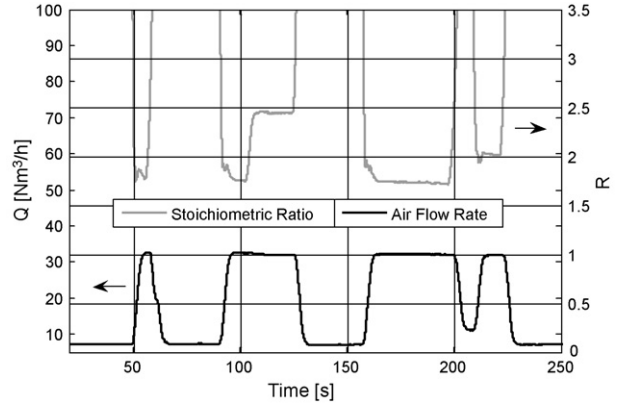

Fig. 12. Stoichiometric ratio and air flow rate vs. time for the experiment of Fig. 11.

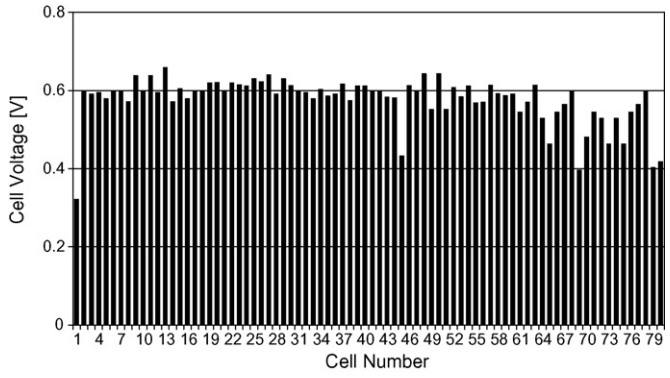

Fig. 14. Individual cell voltage acquisition during the experiment of Fig. 11 at the instant of maximum acceleration (t = 175 s, 230 A).

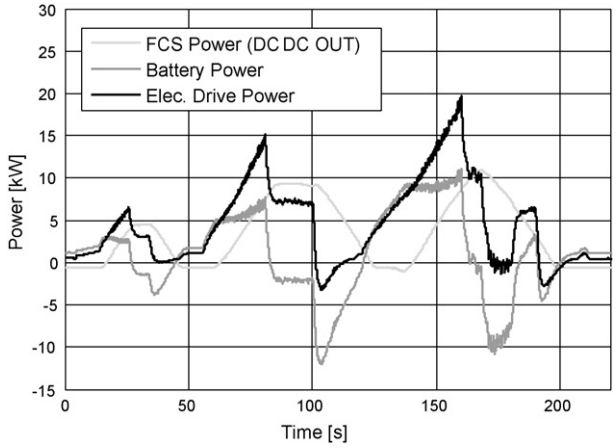

Fig. 15. Power distribution between FCS, electric engine and batteries as function of cycle length for R40 cycle at 5 A s^{-1} as stack current variation rate.

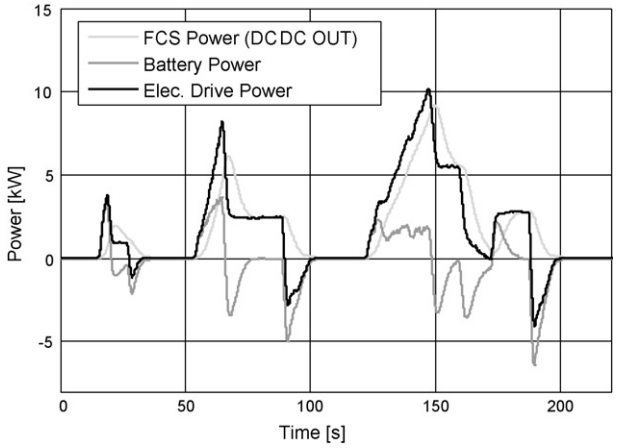

Fig. 16. Power distribution between FCS, electric engine and batteries as function of cycle length for R40 cycle at 10 A s^{-1} as stack current variation rate. Soft hybrid configuration.

on the driving cycle was determined by the following equation, assuming battery efficiency of 100% and taking back the final SOC to the initial level [12]:

$$\eta_{PT} = \eta_{FCS}\eta_{DC}\eta_{ED}$$

For the test of Fig. 15 an efficiency of 46% was obtained for the FCS, which during the cycle operated mainly in conditions of partial loads, characterized by high efficiency [26]. For DC–DC converter and electric drive efficiencies of 78 and 74% were evaluated, respectively, with an overall efficiency value for the power train of about 27%.

Another experiment was performed increasing the slope of the acceleration phases of the R40 cycle, in order to obtain current variations of 10 A s^{-1}, and maintaining the same air management strategy of Fig. 15. The results are shown in Fig. 16, where the power distribution between engine, battery pack and DC–DC converter is reported versus cycle length. For this cycle a different control strategy was adopted, in particular all power requirements from the electric drive were mainly satisfied by the FCS already at the start up, while the contribution of batteries was limited to about 30% of the power demands during acceleration phases. This strategy was chosen according to the soft hybrid option, with the aim of minimizing the intervention of the energy storage devices. The results of Fig. 16 show that the dynamic behaviour of the fuel cell system permitted the energy demands from the engine to be instantaneously satisfied by the stack. The role of batteries in this test was mainly that to allow the energy recovery during the regenerative phases, as evidenced by the negative values reached by battery and engine power curves. The energy recovered during regenerative braking was evaluated and resulted about 15% of the total energy entering into the electric drive during the cycle. The data of Table 1 show that no significant differences were observed in efficiency values for this test with respect to the experiment of Fig. 15, in particular an efficiency value of 26% was calculated for the total power train.

Table 1
Efficiency calculation for the 30 kW fuel cell power train on R40 driving cycle

Efficiencies (%)	Experiment of Fig. 15	Experiment of Fig. 16	Experiment of Fig. 17
η_{FCS}	46	45	48
η_{DC}	78	77	84
η_{ED}	74	74	75
η_{PT}	27	26	30

The hard hybrid configuration was analysed by a test effected on the cycle R40 designed with slope of acceleration phases corresponding to stack current variation rate of 50 A s^{-1}, and a maximum power demand of 35 kW. The results are shown in Fig. 17, where engine power requirements, power contribution of batteries and FCS are reported as function of cycle length for a sequence of three successive cycles. The FCS operated as a power levelling source during the entire cycle (5 kW at the DC–DC converter outlet), while dynamic requirements were provided by batteries. With this strategy the FCS worked in conditions of maximum efficiency, as evidenced by data of Table 1. In particular, the FCS efficiency resulted about 48%, and a significant increase was observed for the DC–DC converter efficiency,

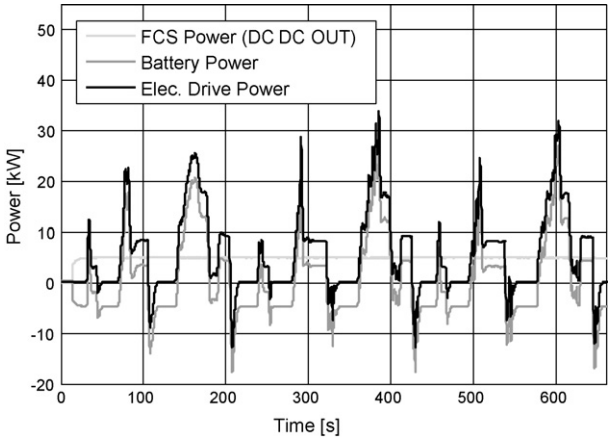

Fig. 17. Power distribution between FCS, electric engine and batteries as function of cycle length for three successive R40 cycles at 50 A s^{-1} and DC–DC output power constant at 5 kW (hard hybrid configuration).

which raised up to 84% with respect to the values calculated for the experiments of Figs. 15 and 16, resulting in an overall power train efficiency of about 30%.

4. Conclusions

The experimental analysis of dynamic performance of a 30 kW fuel cell power train based on 20 kW PEM FCS on test cycles compatible with automotive applications (European R40 driving cycle) permitted the following final remarks to be drawn.

- Air management strategies affected the cell voltage uniformity and fuel cell system efficiency, in particular the best compromise between fuel cell system efficiency and dynamic response in terms of cell voltage uniformity was obtained with an air management strategy characterized by stoichiometric ratio values slightly superior to those optimized for steady state conditions. For stack current variation rates of 50 A s^{-1}, required by the R40 cycle for the reference vehicle considered, the air compressor management did not correspond to the minimum energy consumption condition. In particular, a FCS efficiency diminution of about 2% on the cycle should be considered.
- The hybridization level (soft or hard hybrid configurations) slightly affected the efficiency of single sub-systems and total propulsion system. Passing from soft to hard hybrid the DC–DC converter efficiency varied from 78 to 84%, while FCS efficiency increased from 45 to 48%. As a consequence the maximum total power train efficiency resulted about 30% in hard hybrid configuration, when FCS operated in steady state conditions at power level corresponding to its maximum efficiency, but an efficiency not lower than 26% was obtained for the propulsion system in soft hybrid working.

The indications of this paper suggest that the sizing of a fuel cell power train for minibus applications has to take into account not only efficiency issues, which do not appear determinant in the choice of the hybridization level, but stack durability and costs should be carefully considered. In particular, if the stack dynamic performance resulted suitable for a soft hybrid application, problems connected to stack lifetime should be investigated.

Acknowledgement

The authors gratefully acknowledge Mr Giovanni Cantilena of Istituto Motori for his cooperation in the setup of the experimental apparatus and execution of the tests.

References

[1] J.E. Mason, Energy Policy 35 (2007) 1315–1329.
[2] E.I. Zoulias, N. Lymberopoulos, Renew. Energy 32 (2007) 680–696.
[3] M. Granovskii, I. Dincer, M.A. Rosen, J. Power Sources 157 (2006) 411–421.
[4] M. Granovskii, I. Dincer, M.A. Rosen, Int. J. Hydrogen Energy 31 (2006) 337–352.
[5] J. Larminie, A. Dicks, Fuel Cell Systems Explained, John Wiley & Sons Ltd., Chichester, UK, 2000, pp. 61.
[6] S. Satypal, J. Petrovic, C. Read, G. Thomas, G. Ordaz, Catal. Today 120 (2007) 246–256.
[7] A. Sarkar, R. Banerjee, Int. J. Hydrogen Energy 30 (2005) 867–877.
[8] R. Helmolt, U. Eberle, J. Power Sources 165 (2007) 833–843.
[9] M. Granovskii, I. Dincer, M.A. Rosen, J. Power Sources 159 (2006) 1186–1193.
[10] J. Van Mierlo, G. Maggetto, Ph. Lataire, Energy Conv. Manage. 47 (2007) 2748–2760.
[11] R.K. Ahluwalia, X. Wang, A. Rousseau, R. Kumar, J. Power Sources 130 (2004) 192–201.
[12] M. Ouyang, L. Xu, J. Li, L. Lu, D. Gao, Q. Xie, J. Power Sources 163 (2006) 467–479.
[13] A. Jossen, J. Garche, H. Doering, M. Goetz, W. Knaupp, L. Joerissen, J. Power Sources 144 (2005) 395–401.
[14] P. Thounthong, R. Stephane, B. Davat, J. Power Sources 158 (2006) 806–814.
[15] P. Rodaz, G. Paganelli, A. Sciarretta, L. Guzzella, Control Eng. Pract. 13 (2005) 41–53.
[16] P. Corbo, F.E. Corcione, F. Migliardini, O. Veneri, J. Power Sources 157 (2006) 799–808.
[17] R.A. Costa, J.R. Camacho, J. Power Sources 161 (2006) 1176–1182.
[18] S. Pischinger, C. Schonfelder, J. Ogrzewalla, J. Power Sources 154 (2006) 420–427.
[19] F. Philipps, G. Simons, K. Schiefer, J. Power Sources 154 (2006) 412–419.
[20] S.H. Jung, S.L. Kim, M.S. Kim, Y. Park, T.W. Lim, J. Power Sources 170 (2007) 324–333.
[21] J. Gou, P. Pei, Y. Wang, J. Power Sources 162 (2006) 1104–1114.
[22] P. Corbo, F. Migliardini, O. Veneri, Int. J. Hydrogen Energy 32 (2007) 4340–4349.
[23] R. Cownden, M. Nahon, M.A. Rosen, Int. J. Hydrogen Energy 26 (2001) 615–623.
[24] X. Yu, B. Zhou, A. Sobiesiak, J. Power Sources 147 (2005) 184–195.
[25] R.M. Moore, K.H. Hauer, S. Ramaswamy, J.M. Cunningham, J. Power Sources 159 (2006) 1214–1230.
[26] P. Corbo, F. Migliardini, O. Veneri, Energy Manage. Conv. 48 (2007) 2365–2374.